

## Comparison of density-functional, tight-binding, and empirical methods for the simulation of amorphous carbon

N. A. Marks, N. C. Cooper, and D. R. McKenzie

*School of Physics A28, The University of Sydney NSW 2006, Australia*

D. G. McCulloch, P. Bath, and S. P. Russo

*Department of Applied Physics, RMIT University, GPO Box 2476V, Melbourne VIC 3001, Australia*

(Received 5 July 2001; published 25 January 2002)

Amorphous carbon networks are used to test various levels of theoretical approaches to molecular dynamics simulations. The density-functional theory as implemented in the Car-Parrinello method, nonorthogonal tight-binding method, the environment-dependent interaction potential (EDIP), and the Brenner potential are compared directly in liquid quench simulations containing 125 atoms at four densities. We find that at low densities the predictions of the Brenner potential are in agreement with those from density-functional theory, while structures produced by nonorthogonal tight-binding method compare well with density-functional theory at all densities. The tight-binding method does, however, find a slightly lower  $sp^3$  fraction at high densities and the presence of singly coordinated atoms at low densities. The frequency of three-membered rings are underpredicted by the tight-binding and EDIP methods due to an overestimate of strain energy relative to density-functional theory and experiment. Aside from the small rings, and a slight underestimate in  $sp^3$  fraction at the highest densities, the EDIP simulations are in very good agreement with density-functional theory. The EDIP method is also used to quantify the statistical variability of liquid quenching, and comparisons with film growth simulations verify that liquid quenching is a good representation of bulk amorphous carbon.

DOI: 10.1103/PhysRevB.65.075411

PACS number(s): 61.43.Bn, 02.70.Ns, 81.05.Uw

### I. INTRODUCTION

The diversity of the bonding configurations of the carbon atom makes it an ideal system for testing the transferability of interaction potentials used in molecular dynamics. Interest in amorphous carbon atoms is being stimulated by applications in wear resistance, corrosion resistance and electronics. A wide variety of densities,  $sp^2$  fractions, and mesoscopic structures allow carbon films to be engineered for each application.<sup>1,2</sup>

There has been considerable effort in modeling the structure of amorphous carbon films by molecular dynamics using a rapid liquid quench to simulate the actual formation process from the vapor state. Many different levels of theory<sup>3–11</sup> have been used to describe the interatomic interactions, ranging from density-functional theory, through the various tight-binding approaches, to empirical potential methods. Questions such as stress relief by annealing<sup>12</sup> and the growth of films require long simulation times and/or large system sizes that are not feasible using the more computationally intensive approaches. There is therefore an important role for the more efficient techniques, provided they retain sufficient accuracy to reproduce the correct structure and properties of interest. One of the key aims of this work is to establish which features of the more accurate calculations are retained when lower levels of theory are used.

To investigate these issues we perform liquid-quench simulations of networks using levels of theory that span the variety of techniques available. In order of decreasing accuracy the methods compared are density-functional theory (DFT),<sup>13</sup> the nonorthogonal tight-binding (NOTB) approach,<sup>14</sup> and the empirical environment-dependent interaction potential (EDIP),<sup>15</sup> and Brenner potentials.<sup>16</sup> As far as

is possible the various simulations use identical preparation conditions concerning the number of atoms, density, cooling rate, and coordination cutoff. When comparing structures we calculate bonding and coordination information, radial distribution functions, and ring statistics. Aside from these three-dimensional network calculations we also compute strain energies of a number of ringed hydrocarbon molecules, as previous work has shown<sup>14,17</sup> that the energetics of three- and four-membered rings are dependent on the level of theory and the quality of the basis set.

A further aim of this work is to justify the liquid-quench technique as a means of simulating bulk structure in films grown by vapor condensation. Liquid quenching reproduces the correct time scales of a thermal spike for ion deposition of carbon<sup>18</sup> but differs in detail from the actual processes that occur after energetic impact. An efficient code such as EDIP enables statistical information to be extracted, a knowledge of which is necessary in comparisons between methods.

### Theoretical methods

The DFT method employed in this work is the Car-Parrinello<sup>13,19</sup> implementation of molecular dynamics, which employs a classical description of the motion of the atom cores with a quantum mechanical description of the four valence electrons of each atom as they move in the potential field set up by the cores as represented by pseudopotentials. The wave functions for each electron are described in terms of a plane wave basis set with a cutoff of 40 Ry and the exchange-correlation functional is of the Becke-Lee-Yang-Parr (BLYP) type.<sup>20</sup> Martins-Trouiller pseudopotentials in the Kleinmann-Bylander form<sup>21</sup> were used to represent the carbon ion cores, and were checked for accuracy

against the molecules ethylene, ethane, and ethene, which cover the three main hybridizations of carbon. At a plane wave cutoff of 40 Ry the computed bond lengths fell within 2% of the experimental values.

Tight-binding schemes express the Hamiltonian eigenstates in an atomic-like basis set and parametrize the overlap matrix and the many-body Hamiltonian matrix.<sup>22</sup> The two-center NOTB scheme of Porezag *et al.*<sup>14</sup> used here employs density-functional calculations to tabulate the required parameters, and an exact  $k$ -space diagonalization calculation of the tight-binding energy.

The Brenner empirical potential<sup>16</sup> was designed to account for changes in atomic hybridization during bond breaking and formation in hydrocarbons. Based on the bond order approach of Tersoff,<sup>23</sup> this potential was developed in order to describe the different possible bonding states in carbon more correctly than that predicted by the Stillinger-Weber<sup>24</sup> or Tersoff potentials. The Brenner potential has recently been extended to Si-C-H systems<sup>25</sup> and has been used to model chemically vapor deposited (CVD) diamond films<sup>16</sup> and indentation at diamond surfaces.<sup>26</sup>

The EDIP is a new addition to carbon simulation methods. First proposed for silicon,<sup>27</sup> it was recently generalized for carbon<sup>15</sup> and has been found to provide high transferability for comparatively low computational cost. The usefulness of the EDIP approach was demonstrated in recent simulations of thin film growth<sup>28</sup> where tetrahedral amorphous carbon was deposited using energetic beams for the first time.

## II. THE LIQUID QUENCH

The amorphous carbon structures considered in this study are prepared experimentally by condensing hyperthermal atoms onto a substrate held at a temperature below approximately 400 K. A molten region surrounds the impact site of incident atoms for a short time after impact. Calculations<sup>18</sup> show that such thermal spikes are quenched in a fraction of a picosecond, enabling molecular dynamics to provide realistic simulations of the formation process. In a liquid-quench simulation the short-lived thermal spike is modeled by rapidly cooling a molten sample to room temperature. In the case of carbon, generation of the liquid sample is commonly achieved by way of a simple cubic lattice, an unstable structure that spontaneously melts. After equilibration at 5000 K, the amorphous network is formed by quenching the liquid to 300 K in a time  $t_0$  along a cooling curve typically either exponential or linear. Thermally averaged properties are then computed at 300 K.

Following this procedure a large number of liquid-quench calculations were performed using EDIP in simulations at 2.9 g/cm<sup>3</sup>. The liquid was equilibrated for 0.8 ps, and from this sample 100 simulations were undertaken for each system considered, with each quench using a slightly different configuration for the equilibrated liquid. This was achieved by saving the liquid state point prior to each cooling cycle, and then allowing the liquid to evolve for 0.1 ps prior to the subsequent quench. Systems with 64 and 125 atoms were cooled exponentially with  $t_0=0.5$  ps, while a third simulation set contained 125 atoms and was linearly cooled with

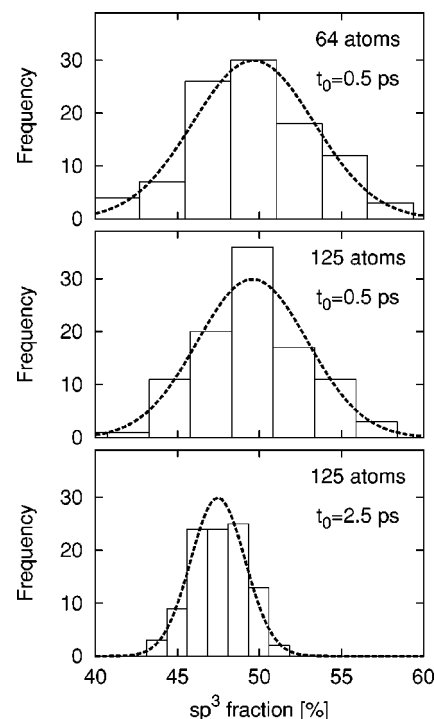


FIG. 1. Distribution of  $sp^3$  fractions in liquid-quench simulations carried out in 64- and 125-atom systems. 100 quenches were performed for each system and the density was 2.9 g/cm<sup>3</sup>. Cooling curves for the 0.5 ps and 2.5 ps quenches were exponential and linear, respectively. Dotted lines indicate the normal distribution with mean and standard deviation of the data sets. The coordination was determined using a bond cutoff of 1.85 Å.

$t_0=2.5$  ps. These three systems are generally representative of liquid-quench calculations in the amorphous carbon literature.

Figure 1 indicates the statistical variation in the  $sp^3$  fraction of the equilibrated structures for the three scenarios considered. This statistical uncertainty is much larger than previously acknowledged, and represents an important factor to consider when comparing different preparation conditions and methods. The variability arises from fluctuations in the liquid state at the instant the quench is initiated, and the metastable nature of the rapidly quenched structures. Both of these factors are an intrinsic part of the experimental deposition process, and are not artifacts of the simulation technique. System size is not a key factor determining the  $sp^3$  fraction, as the 64- and 125-atom simulations cooled in 0.5 ps have very similar distributions. Analysis using the null hypothesis finds that the mean value of both 0.5 ps simulations came from the same distribution, confirming the absence of a statistically significant difference.

The cooling rate, however, does make a difference to the observed  $sp^3$  fractions. A paired difference analysis of the two 125-atom simulation sets is possible as the  $n$ th quench in each set uses the same liquid starting configuration. This analysis yields a difference of 1.8–3.2 at the 95% confidence interval, and helps interpret a number of DFT simulations examining the effect of the cooling rate. In 64-atom simulations at 2.9 g/cm<sup>3</sup>, Marks *et al.*<sup>4</sup> found that the  $sp^3$  fraction

TABLE I. Mean and standard deviation (SD) for structural parameters in the EDIP liquid-quench simulations presented in Fig. 1. The coordination is determined by counting neighbors within 1.85 Å.  $R_{\text{av}}$  and  $\theta_{\text{av}}$  are the average nearest-neighbor distance and average bond angle, respectively.  $\Delta R$  and  $\Delta\theta$  describe the standard deviations of the distances and angles, respectively. The number of rings of length six are computed using the algorithm of Franzblau (Ref. 35).

Quantity	64/0.5 ps		125/0.5 ps		125/2.5 ps	
	Mean	SD	Mean	SD	Mean	SD
$sp^3$ (%)	49.6	3.7	49.6	3.4	47.5	1.7
$R_{\text{av}}$ (Å)	1.550	0.010	1.546	0.008	1.544	0.007
$\Delta R$ (Å)	0.093	0.006	0.092	0.005	0.086	0.004
$\theta_{\text{av}}$ (deg)	111.38	0.33	111.41	0.23	111.39	0.20
$\Delta\theta$ (deg)	10.01	0.60	9.95	0.45	9.30	0.36
No. (six-member ring)	18.0	6.3	39.2	7.6	43.6	8.0

decreased from 68% to 57% as the quenching time increased, while 125-atom simulations at 3.2 g/cm<sup>3</sup> found an  $sp^3$  fraction of 80.1 and 80.3 for  $t_0$  values of 0.5 and 1.0 ps, respectively. Further 64-atom simulations<sup>29</sup> at 2.9 g/cm<sup>3</sup> with in principle the same preparation conditions as the 65%  $sp^3$  sample in Ref. 4 found an  $sp^3$  fraction of  $\approx 55\%$ . These disparate results can be understood in the context of the statistical variability evident in Fig. 1. All of the DFT results lie within the statistical range found using EDIP, and while a cooling rate effect is present, it not nearly is pronounced as presumed in Ref. 4.

As might be anticipated from the  $sp^3$  data, other quantities in a liquid quench are also subject to significant statistical variation. Nearest-neighbor distances, bond angles, and ring statistics are all important quantities when comparing amorphous networks, and their variation is indicated in Table I. The standard error in the mean (SEM) is defined as  $\sigma/\sqrt{n}$  and so with  $n = 100$  simulations in each category the SEM is one-tenth of the standard deviation  $\sigma$ . Comparison using the SEM indicates that the similarity between the two 0.5 ps quenches extends to virtually all the quantities considered, with only the most minor of differences evident in the nearest neighbor distance.

An important insight from Table I is the reduction in amorphicity when the cooling time is increased. In addition to the much narrower distribution of  $sp^3$  fractions, the slowest cooling also gives rise to the smallest values of  $\Delta\theta$  and the greatest number of rings. These differences are all significant at the 99.7% level due to the high precision in the SEM. The large number of six-membered rings is particularly important, as this occurs against the general trend seen in simulations at varying density whereby a smaller  $sp^3$  fraction means fewer rings due to lower connectivity. Together with the reduced spread in bond angles, this illustrates the concept of accessibility in nonequilibrium situations as described by McKenzie and Bilek.<sup>30</sup> The key idea is that the thermodynamic arrow can only be followed to completion if sufficient temperature and time are available. In these simulations it is clear that more crystalline-like properties are obtained when the system is given a longer time to move towards the global minima. In the limit of very long cooling times (perhaps 1 ns) it is also reasonable to postulate that, for

each density, a thermodynamically stable structure of amorphous carbon exists, independent of the quenching time.

Figure 2 shows the uncertainty in the ring statistics, with the error bars indicating the one standard deviation limits. For the larger rings in particular, the signal is almost swamped by the noise, and while the confidence interval for the mean as determined by the SEM is much smaller, this is not especially helpful when comparing single-run simulations as generally encountered in the literature. In these cases the uncertainty is of the order of the error bars shown in Fig. 2 and perhaps higher, and hence care must be taken when drawing conclusions. The level of noise in ring statistics data is illustrated by the graphical comparison between DFT and EDIP in Ref. 15, where although the agreement is not quantitative for individual ring size, overall there is excellent qualitative agreement for rings of length five and higher. Another factor when comparing methods is that ring statistics are somewhat computationally expensive to compute, and so are often determined only at the end of a simulation run. This absence of thermal averaging contributes additional statistical noise if bond lengths at 300 K are fluctuating around the coordination cutoff.

We conclude this section with a comparison of liquid-quench data with as-deposited thin films. Although the

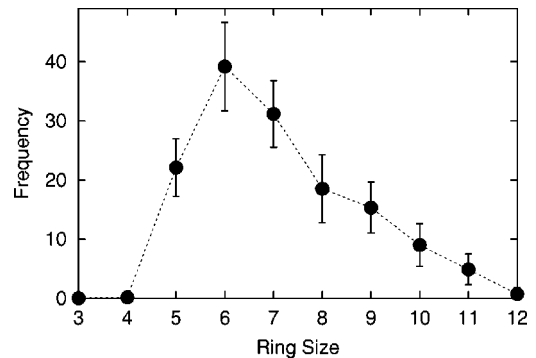


FIG. 2. Distribution of rings for 100 liquid quenches in the 125-atom system with  $t_0 = 0.5$  ps and exponential cooling. Error bars indicate the standard deviation of the distribution. The 95% confidence interval for the mean frequency is approximately the size of the solid circles.

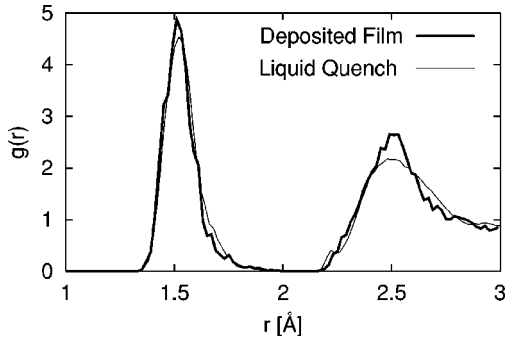


FIG. 3. Radial distribution function  $g(r)$  for EDIP simulations of liquid quenching (this work) and thin film deposition (Ref. 28). The quench simulation was performed at  $3.2 \text{ g/cm}^3$ , while the film was deposited with a 40 eV beam. The as-deposited  $g(r)$  refers to the bulk region of the film, where the density was  $3.17 \text{ g/cm}^3$ .

liquid-quench method is justified by inference and analytic calculations,<sup>18</sup> there has yet to be a simulation proving that liquid quenching provides a good description of the bulk region in amorphous carbon deposited with energetic beams. Recent EDIP simulations of carbon thin film growth<sup>28</sup> enable such a comparison for the first time. The film growth simulations involved the deposition of 500 atoms onto a reconstructed (100) diamond substrate at 300 K. For each impact full dynamics were followed for 0.5 ps, and rethermalization to 300 K was performed prior to the deposition of the subsequent atom. The films were all amorphous and steady state growth was quickly attained, enabling a straightforward identification of the bulk region of the film. A number of films were deposited, with energies varying between 1 and 100 eV. Figure 3 compares the pair distribution function of tetrahedral amorphous carbon (*ta*-C) prepared by EDIP liquid quench at  $3.2 \text{ g/cm}^3$  with that of bulk *ta*-C deposited with a 40 eV atomic beam. The structures in the two simulations have very similar distributions of distances despite the different preparation conditions. Note also that although both structures have essentially the same density ( $3.2 \text{ g/cm}^3$ ), the density in the quench is an input parameter, whereas it is an output quantity in the deposition.

The close agreement between liquid quenching and deposited amorphous carbon extends to the  $sp^3$  fraction, whose dependence on density is shown in Fig. 4. Shown in this figure are the  $sp^3$  fractions for the thin film deposition simulations (white circles), and the same quantity from additional liquid-quench simulations at 2.0, 2.3, 2.6, and  $3.2 \text{ g/cm}^3$  (black circles). The additional liquid-quench data represent an average over 25 simulations. Across a broad density range, the  $sp^3$  fraction of the quenched structures shares the same linear dependence as the films deposited at varying energy. The simulations are consistent with experiments<sup>31</sup> that show that the  $sp^3$  fraction is a single-valued function of the density as seen in Fig. 4. The simplest analysis of this experimental data yielded a straight line, but the uncertainties were too great to eliminate the possibility of nonlinear relationship between the  $sp^3$  fraction and the density as suggested by Lossy *et al.*<sup>32</sup> However, with the precision afforded by the multiple liquid-quench simulations the linear relationship is affirmed. The importance of statistical variation is

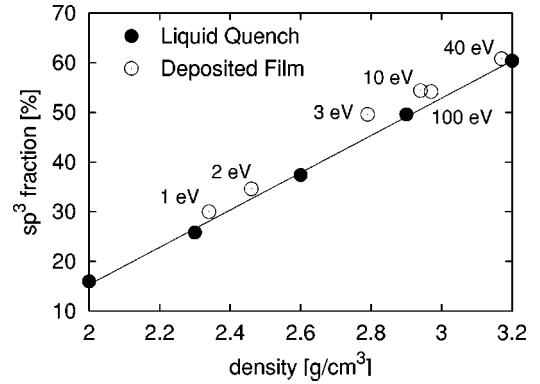


FIG. 4. Variation in  $sp^3$  fraction with density in EDIP simulations of liquid quench (this work) and deposition simulations (Ref. 28). The labels in eV indicate the beam energy used to deposit each film. All of the liquid-quench points are an average of at least 25 simulations, and the uncertainty in the mean is smaller than the data point. The solid line is a linear fit to the quench data.

further highlighted by the first EDIP liquid-quench simulations<sup>15</sup> where the variation of  $sp^3$  fraction with density is not a straight line because only a single quench was performed at each density.

### III. COMPARISON OF TECHNIQUES

Having established a statistical basis for comparison of methods, we now use 125-atom simulations of carbon at four densities using the chosen levels of theory. A liquid was prepared by melting an unstable simple cubic structure and equilibrating it at 5000 K for 0.5 ps. Then the final network was formed by quenching the liquid along an exponential cooling curve of the form  $T(t) = 5000e^{-ct}$ . Structures were produced at all four densities by cooling to 300 K in 0.5 ps. The dynamics of the systems were followed at 300 K for at least an additional 500 fs to enable structural properties to be determined.

Figure 5 compares the reduced density function  $G(r)$  for the DFT and EDIP simulations with experimental neutron diffraction data. The DFT simulations are in good agreement with experiment, and are used in the remainder of this work as the benchmark against which to evaluate the other simulations. It is also evident that the EDIP simulations reproduce to a high degree of accuracy the features of the DFT simulations. This agreement extends the already good predictive properties of EDIP with regard to coordination fractions, bond angles, ring statistics, and melting properties.<sup>15</sup>

Figure 6 compares the same DFT data with the results of the NOTB and Brenner potential simulations. The DFT and NOTB calculations are in good agreement over a wide range of densities, while the Brenner potential agrees at low density, but at higher densities deviates in its detail and the position of the first nearest neighbor. The sharp peak at  $1.22 \text{ \AA}$  in the DFT and NOTB calculations at  $2.0 \text{ g/cm}^3$  is consistent with the work of Stephan *et al.*<sup>7</sup> who found low coordinated atoms with a short bond length of  $1.23 \text{ \AA}$ , which they described as “triplelike.”

The peaks in the Brenner calculations around  $2.0 \text{ \AA}$  are

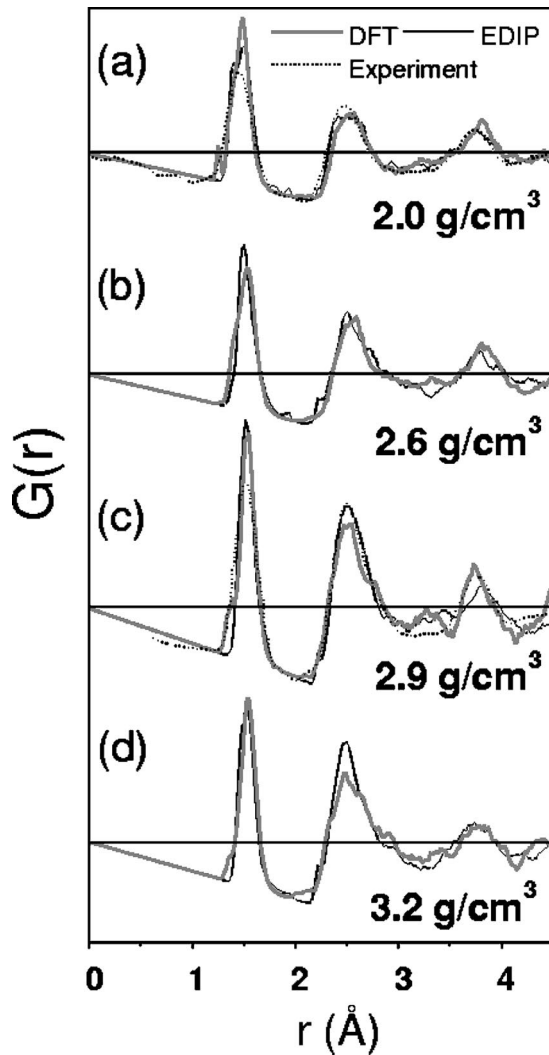


FIG. 5. The reduced density function  $G(r)$  calculated from the networks produced using DFT and EDIP at densities of (a) 2.0, (b) 2.6, (c) 2.9, and (d) 3.2  $\text{g/cm}^3$ . The experimental data are from Li and Lannin (2.0  $\text{g/cm}^3$ ) (Ref. 37) and Gilkes *et al.* (2.9  $\text{g/cm}^3$ ) (Ref. 38).

particularly noteworthy as they represent a metastable state intermediate between graphite and diamond. Similar spikes were found by Jäger and Albe<sup>33</sup> in their simulations of energetic carbon deposition using Tersoff and modified Brenner potentials. In both sets of simulations large spikes in the pair distribution function were observed at the interaction cutoff distance, the same behavior as observed here where the Brenner cutoff is 2.05 Å.

The structural parameters of nearest-neighbor distances, average bond angle, and coordination percentages are shown in Table II. The DFT, NOTB, and EDIP simulations are all generally similar in their predictions, with the higher level of theory in NOTB correlating to slightly close agreement with DFT, particular at the highest density. The exception to this trend is NOTB simulation at 2.0  $\text{g/cm}^3$ , which contains 5% singly coordinated atoms indicating a dangling bond. Several of these singly coordinated atoms are associated with the short bond distance of 1.22 Å seen in Fig. 6. However, when

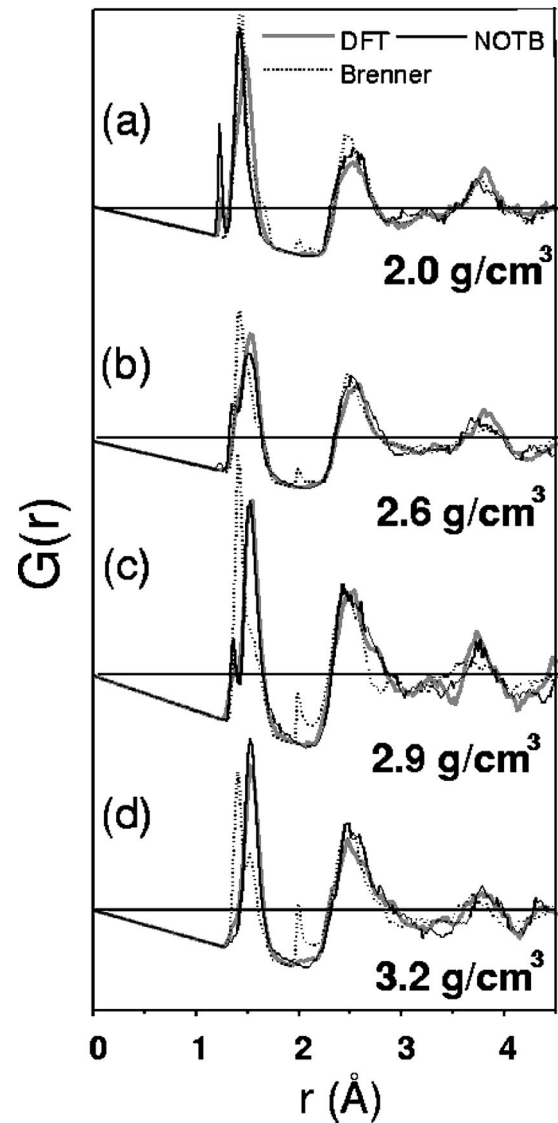


FIG. 6. The reduced density function  $G(r)$  calculated from the networks produced using DFT, NOTB, and Brenner potential methods at densities of (a) 2.0, (b) 2.6, (c) 2.9, and (d) 3.2  $\text{g/cm}^3$ .

these short bond distances are present in the DFT simulations they are not associated with singly coordinated atoms. These short distances contribute to an overly short nearest-neighbor distance in the 2.0  $\text{g/cm}^3$  structure as manifested in the peak offset in Fig. 6.

The Brenner potential gives results in close agreement with DFT at the lowest density, with bond lengths, angles, and coordination numbers all comparing well. However, there is an increasing departure from the DFT results as the density rises. This reflects the methodology of the Brenner potential whereby the functional form was performed with surfaces and molecules in mind. Unlike EDIP, there is no energy penalty for nonbonded  $\pi$  interactions, and hence graphitelike structures can have unphysically high densities close to that of diamond. Consequently the Brenner potential lacks the driving force to convert  $sp^2$  sites into  $sp^3$ , resulting in the low fraction of fourfold coordinate atoms seen in Table II.

TABLE II. Structural parameters from liquid-quench simulations with  $t_0=0.5$  ps and exponential cooling. Average bond length, average bond angle, and coordination numbers are all determined by counting neighbors within 1.85 Å. EDIP values are averages over at least 25 simulations, while a single calculation was performed with the other methods.

Density (g/cm <sup>3</sup> )	Method	$r$ (Å)	Bond angle (deg)	Coordination			
				$C_1$	$C_2$	$C_3$	$C_4$
2.0	DFT	1.48	119.3	0	15	77	8
2.0	NOTB	1.43	122.0	5	29	60	6
2.0	EDIP	1.49	115.4	0	21	63	16
2.0	Brenner	1.49	118.2	0	16	70	14
2.6	DFT	1.53	112.2	0	1	56	43
2.6	NOTB	1.51	114.2	0	8	60	32
2.6	EDIP	1.54	112.3	0	4	59	37
2.6	Brenner	1.50	116.0	0	2	80	18
2.9	DFT	1.54	111.1	0	1	41	58
2.9	NOTB	1.54	111.6	0	1	49	50
2.9	EDIP	1.55	111.4	0	1	49	50
2.9	Brenner	1.49	115.5	0	2	79	19
3.2	DFT	1.55	109.7	0	0	19	81
3.2	NOTB	1.55	109.7	0	2	23	75
3.2	EDIP	1.53	110.8	0	0	39	61
3.2	Brenner	1.48	115.7	0	4	75	21

A comparison in Fig. 7 of the simulations with experiment reveals a linear variation in  $sp^3$  fraction with density, consistent with experiment and the EDIP results of Fig. 4. The DFT data show the closest agreement with experiment, with NOTB underestimating DFT by an average of 7%. In light of the liquid-quench variability demonstrated by EDIP it is necessary to apply statistical procedures to quantify this difference. A one-side paired  $t$  test finds a  $p$  value of 0.019, indi-

cating a statistically significant underestimation of the DFT data by NOTB. EDIP also underestimates DFT at high densities. At 2.9 g/cm<sup>3</sup> it is more than 95% likely that the DFT value of 58% does not come from the EDIP distribution in Fig. 1, while at 3.2 g/cm<sup>3</sup> where the standard deviation is 2.1 the underestimation is even more significant.

The discrepancy with respect to DFT is most serious for the Brenner potential, where the  $sp^3$  fraction is seriously underestimated with increasing density as noted earlier.

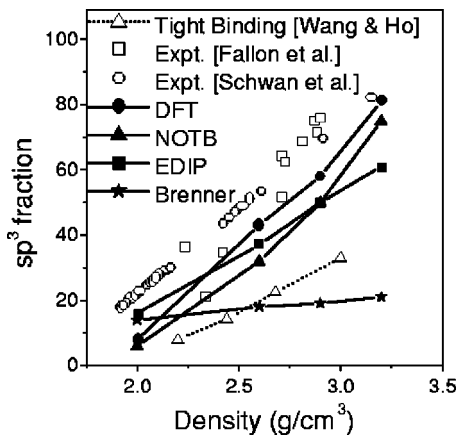


FIG. 7. The  $sp^3$  fraction plotted as a function of density calculated from the networks produced using the DFT, NOTB, EDIP, and Brenner potential methods in this work (filled symbols). Open triangles indicate the orthogonal tight-binding calculations of Wang and Ho (Ref. 10). Open circles are experimental results from argon/carbon magnetron sputtered amorphous carbon (Ref. 39). Open squares are experimental values from ion-beam deposited amorphous carbon (Ref. 31).

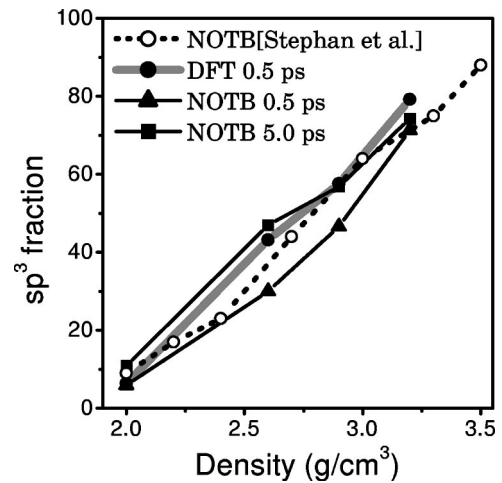


FIG. 8. The  $sp^3$  fraction plotted as a function of density calculated from the networks produced using NOTB with quench times of 0.5 and 5.0 ps. Also shown is the results from the DFT simulations with a quench time of 0.5 ps. The open circles are the results from the NOTB calculations of Stephan *et al.* (Ref. 7).

TABLE III. The distribution of ring sizes in each of the networks produced. The procedure for calculating ring sizes is based on the method of Franzblau (Ref. 35). The EDIP values are averaged over at least 25 simulations, while a single calculation was performed with the other methods.

Density (g/cm <sup>3</sup> )	Method	Number of Rings									
		3	4	5	6	7	8	9	10	11	12
2.0	DFT	2	3	13	6	1	5	5	4	12	2
2.0	NOTB	0	0	6	11	4	2	1	3	3	5
2.0	EDIP	0	1	14	13	10	5	5	4	4	4
2.0	Brenner	4	1	7	13	10	10	3	4	10	2
2.6	DFT	7	7	21	19	15	18	15	17	6	3
2.6	NOTB	0	2	19	33	14	13	4	15	6	2
2.6	EDIP	0	1	22	30	21	16	12	9	6	1
2.6	Brenner	4	0	5	10	13	23	22	12	22	5
2.9	DFT	2	6	31	42	25	21	21	2	5	0
2.9	NOTB	0	3	32	42	16	11	6	12	7	0
2.9	EDIP	0	0	22	39	31	19	15	9	5	1
2.9	Brenner	1	0	9	14	16	22	12	19	13	4
3.2	DFT	3	11	37	53	49	26	23	3	2	0
3.2	NOTB	3	5	38	58	47	19	8	9	0	0
3.2	EDIP	0	0	21	65	41	25	15	9	3	0
3.2	Brenner	0	0	6	18	11	18	25	18	11	4

Similar behavior has been found with the Tersoff potential<sup>11,34</sup> with  $sp^3$  fractions of just 34% at a density of 3 g/cm<sup>3</sup>. Also shown in the figure are the orthogonal tight-binding (OTB) results of Wang and Ho<sup>10</sup> that are coincident with the Tersoff calculations at high densities. It is evident that the Tersoff, Brenner, and OTB methods are unsuitable for modeling tetrahedral amorphous carbon as an abundance of tetrahedral bonding is not observed at high density.

Across the five methods shown in Fig. 7 there is almost complete correlation between computational cost, the level of theory, and the agreement with experiment. The exception to this rule is EDIP, which provides transferability approaching NOTB while being more than 20 times faster than the OTB method, which considerably underpredicts the tetrahedral properties.

Four additional NOTB simulations (one at each density) were performed with much longer quenching times, using linear cooling over 5.0 ps. This enables much greater configurational flexibility during the quench, and the results shown in Fig. 8 suggest a systematic dependence of  $sp^3$  fraction on the quench time opposite to that found in DFT and EDIP simulations. A one-sided paired  $t$  test shows that the difference between the two quench schemes is significant with a  $p$ -value of 0.033. With this much longer quench time the NOTB results approach the DFT data obtained at short quench times. The  $sp^3$  fractions in the 5.0 ps quench also agree well with the NOTB calculations of Stephan *et al.*,<sup>7</sup> who also used a relatively long quench time. The dependence on quench time observed in the case of NOTB is consistent with a general overestimate of energy barriers within the system. Since EDIP is parametrized to the DFT description of the intermediate states between graphite and diamond, the energy barriers for  $sp^2$ - $sp^3$  interconversion are the same,

explaining the similar quench time dependence. NOTB, on the other hand, will overestimate the  $sp^2$ - $sp^3$  barrier because of the absence of states with  $d$  orbital symmetry in the Hamiltonian.

Ring statistics were calculated using the shortest path criteria of Franzblau<sup>35</sup> and a bonding cutoff of 1.85 Å. The results shown in Table III demonstrate that DFT, NOTB, and EDIP give similar ring statistics over the complete density range, particularly in light of the statistical variability seen in Fig. 2. The only exception concerns rings of length three and four, where NOTB and EDIP both underpredict DFT, particularly with regard to the highly strained three-membered

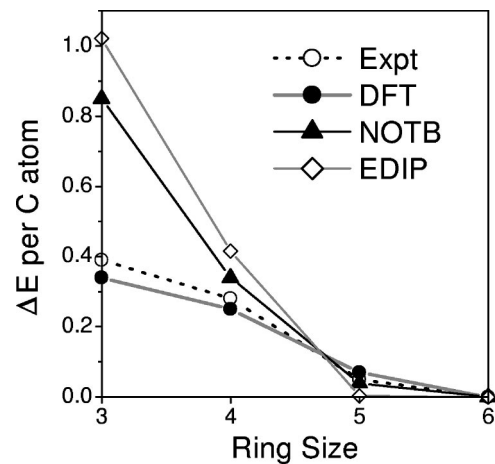


FIG. 9. The strain energy associated with forming three-, four-, and five-membered rings in the cycloalkanes calculated using DFT and NOTB methods compared to experiment (Ref. 36). The EDIP values indicate an equivalent energy cost for pure carbon.

ring. It is interesting to note that the highest-density NOTB calculation contains three-membered rings, and to the best of our knowledge these rings have not previously been reported. We should point out, however, that using a slightly smaller coordination cutoff of 1.80 Å caused these three-membered rings to disappear from the statistics, so these NOTB rings should not be confused with the DFT calculations where the bond length in a three-membered ring is typically 1.5–1.6 Å. The Brenner potential, on the other hand, gives good agreement with the DFT result at low densities, finding both three- and four-membered rings. However, as the density increases the Brenner structures show too few rings since links via  $sp^3$  bonded atoms are low in number. The good agreement shown by the Brenner potential at low densities arises from the parametrization data set, which includes the highly strained cyclopropane and cyclobutane. Since these strain molecules are well described, the correct ring statistics follow.

Small molecule calculations were also performed to determine the strain energy associated with forming three-, four-, and five-membered rings. This was achieved by computing the energy per carbon atom in the three molecules cyclopropane, cyclobutane, and cyclopentane relative to cyclohexane (assumed strain free). The results are shown in Fig. 9, where we compare against experimental values.<sup>36</sup> Reasonable agreement is found for both DFT and NOTB for the four- and five-membered rings. However, in the case of the three-membered ring, NOTB overestimates the strain energy by well over a factor of 2. This observation explains the small number of three-membered rings in the networks produced using NOTB. The overestimation of the strain energy of three-membered rings has been noted previously using NOTB<sup>14</sup> and other first-principles calculations with limited basis sets.<sup>17</sup> Since the frequency of occurrence of three-membered rings in amorphous carbon networks will be strongly dependent on their energetics, we conclude that DFT with a sufficiently large plane-wave basis more accurately reproduces the ring size distribution in real networks than the NOTB method.

Figure 9 also includes an estimate of the EDIP strain energy, using pure carbon rings and a coordination  $Z$  for each atom of  $Z=2+\sum f(r)$  in the notation of Ref. 15. This approximate approach compensates for the absence of a hydro-

gen term in EDIP, with the *ad hoc* value of 2 accounting for the effect of the hydrogen on the carbon hybridization state. The behavior of EDIP is close to that of NOTB, with slightly higher penalties for the two smallest rings. This explains the absence of the three-membered rings in Table IV, although it should be noted that the occasional EDIP simulation at low densities did contain a three-membered ring, consistent with the statistical variability of liquid quenching.

#### IV. CONCLUSION

This evaluation of DFT, NOTB, EDIP, and Brenner molecular dynamics simulations of carbon networks has shown the following:

(1) The properties of structures generated by picosecond liquid quenching have an intrinsic statistical distribution that must not be overlooked when comparing methods and preparation conditions.

(2) The generation of amorphous networks by liquid quenching yields structures in very good agreement with those formed by ion-beam deposition.

(3) The Brenner potential works well at low densities but shows strong deviation at high densities.

(4) The EDIP method shows good overall agreement with DFT, with the most significant differences found in the frequency of small rings, and a slight underestimate of  $sp^3$  fraction at high density.

(5) The NOTB method gives a higher energy for a three-membered ring than does DFT, which explains their comparative absence in NOTB generated networks compared to DFT structures.

(6) At low densities, the NOTB method predicts singly coordinated atoms not observed in the DFT, EDIP, and Brenner simulations.

(7) A dependency on quench rate was observed in the case of NOTB, which may be explained by limitations in the basis set used to describe intermediate bonding states.

In summary, whilst DFT is the most transferable method, NOTB can be used effectively to minimize computation time provided that its limitations in special configurations are recognized. EDIP provides excellent transferability for an empirical potential, while the Brenner potential is only effective at low densities.

<sup>1</sup>J. Robertson, *Adv. Phys.* **35**, 317 (1986).

<sup>2</sup>D.R. McKenzie, *Rep. Prog. Phys.* **59**, 1611 (1996).

<sup>3</sup>G. Galli, R.M. Martin, R. Car, and M. Parrinello, *Phys. Rev. B* **42**, 7470 (1990).

<sup>4</sup>N.A. Marks, D.R. McKenzie, B.A. Pailthorpe, M. Bernasconi, and M. Parrinello, *Phys. Rev. Lett.* **76**, 768 (1996); *Phys. Rev. B* **54**, 9703 (1996).

<sup>5</sup>D.G. McCulloch, D.R. McKenzie, and C.M. Goringe, *Phys. Rev. B* **61**, 2349 (2000).

<sup>6</sup>D.A. Drabold, P.A. Fedders, and P. Stumm, *Phys. Rev. B* **49**, 16 415 (1994).

<sup>7</sup>U. Stephan, Th. Frauenheim, P. Blaudeck, and G. Jungnickel,

*Phys. Rev. B* **50**, 1489 (1994).

<sup>8</sup>Th. Frauenheim, P. Blaudeck, U. Stephan, and G. Jungnickel, *Phys. Rev. B* **48**, 4823 (1993).

<sup>9</sup>Th. Frauenheim, G. Jungnickel, U. Stephan, P. Blaudeck, S. Deuschmann, M. Weiler, S. Sattel, K. Jung, and H. Ehrhardt, *Phys. Rev. B* **50**, 7940 (1994).

<sup>10</sup>C.Z. Wang and K.M. Ho, *Phys. Rev. B* **50**, 12 429 (1994).

<sup>11</sup>U. Stephan and M. Haase, *J. Phys.: Condens. Matter* **5**, 9157 (1993).

<sup>12</sup>T. Friedmann, J.P. Sullivan, J.A. Knapp, D.R. Tallant, D.M. Follstaedt, D.L. Medlin, and P.B. Mirkarimi, *Appl. Phys. Lett.* **71**, 3820 (1997).

- <sup>13</sup>R. Car and M. Parrinello, Phys. Rev. Lett. **55**, 2471 (1985).
- <sup>14</sup>D. Porezag, Th. Frauenheim, Th. Kohler, G. Seifert, and R. Kaschner, Phys. Rev. B **51**, 12 947 (1995).
- <sup>15</sup>N. A. Marks, Phys. Rev. B **63**, 035401 (2001).
- <sup>16</sup>D.W. Brenner, Phys. Rev. B **42**, 9458 (1990); Phys. Status Solidi B **217**, 23 (2000).
- <sup>17</sup>P. A. Schultz and E. B. Stechel, Phys. Rev. B **57**, 3295 (1998); P. A. Schultz, K. Leung, and E. B. Stechel, *ibid.* **59**, 733 (1999).
- <sup>18</sup>N.A. Marks, Phys. Rev. B **56**, 2441 (1997).
- <sup>19</sup>J. Hutter, A. Alavi, T. Deutsch, M. Bernasconi, St. Goedecker, D. Marx, M. Tuckerman, and M. Parrinello, CPMD Code, MPI fur Festkorperforschung and IBM Zurich Research Laboratory 1995–1999.
- <sup>20</sup>A. D. Becke, Phys. Rev. A **38**, 3098 (1988); C. Lee, W. Yang, and R.G. Parr, Phys. Rev. B **37**, 785 (1998).
- <sup>21</sup>L. Kleinman and D.M. Bylander, Phys. Rev. Lett. **48**, 1425 (1982).
- <sup>22</sup>C.M. Goringe, D.R. Bowler, and E. Hernandez, Rep. Prog. Phys. **60**, 1447 (1997).
- <sup>23</sup>J. Tersoff, Phys. Rev. B **39**, 5566 (1989).
- <sup>24</sup>P. Mahon, B.A. Pailthorpe, and G.B. Bacskey, Philos. Mag. B **63**, 1419 (1991).
- <sup>25</sup>A.J. Dyson and P.V. Smith, Surf. Sci. **355**, 140 (1996).
- <sup>26</sup>J.A. Harrison, C.T. White, R.J. Colton, and D.W. Brenner, Surf. Sci. **271**, 57 (1992).
- <sup>27</sup>J. F. Justo, M. Z. Bazant, E. Kaxiras, V. V. Bulatov, and S. Yip, Phys. Rev. B **58**, 2539 (1998).
- <sup>28</sup>N.A. Marks, J. Phys: Condens. Matter (to be published).
- <sup>29</sup>D.G. McCulloch (unpublished).
- <sup>30</sup>D.R. McKenzie and M.M.M. Bilek, Thin Solid Films **382**, 280 (2001).
- <sup>31</sup>P.J. Fallon, V.S. Veerasamy, C.A. Davis, J. Robertson, G.A.J. Amaratunga, W.I. Milne, and J. Koskinen, Phys. Rev. B **48**, 4777 (1993).
- <sup>32</sup>R. Lossy, D. L. Pappas, R. A. Roy, J. P. Doyle, J. J. Cuomo, and J. Bruley, J. Appl. Phys. **77**, 4750 (1995).
- <sup>33</sup>H. U. Jäger and K. Albe, J. Appl. Phys. **88**, 1129 (2000).
- <sup>34</sup>M. Kaukonen and R.M. Nieminen, Phys. Rev. B **61**, 2806 (2000).
- <sup>35</sup>D.S. Franzblau, Phys. Rev. B **44**, 4925 (1991).
- <sup>36</sup>*CRC Handbook of Chemistry Physics* (CRC Press, Boca Raton, FL, 1985).
- <sup>37</sup>F. Li and J. S. Lannin, Phys. Rev. Lett. **65**, 1905 (1990).
- <sup>38</sup>K. W. R. Gilkes, P. H. Gaskell, and J. Robertson, Phys. Rev. B **51**, 12 303 (1995).
- <sup>39</sup>J. Schwan, S. Ulrich, T. Theel, H. Roth, H. Ehrhardt, P. Becker, and S.R.P. Silva, J. Appl. Phys. **82**, 6024 (1997).